

Milliradian-phase-resolution atom interferometer with transparent electrodes for measurement of the Röntgen phase

Taku Kumiya, Alexander S. Akentyev,* Yoshihiro Mori, Junya Ichimura, and Atsuo Morinaga†

Department of Physics, Faculty of Science and Technology, Tokyo University of Science, 2641 Yamazaki, Noda, Chiba 278-8510, Japan

(Received 9 October 2015; published 24 February 2016)

An atom interferometer with a milliradian phase resolution was realized using a subhertz linewidth diode laser. The Allan deviation of the phase fluctuation decreased according to $\sigma/\text{mrad} = 70/\sqrt{\tau}/\text{s}$ and reached 1 mrad at an integration time of 5000 s. With the transparent electrodes with a transmittance of 97%, the visibility of the interference was 8.5%, which was almost the same size as that with zero electric field. The dependence of the phase on the laser frequency was $0.1 \mu\text{rad}/\text{Hz}$ and that on the electric field was 1 mrad for $0.1 \text{ V}/\text{cm}$. Using the transition between the $^3P_1, m = 0$ and $^1S_0, m = 0$ states of Ca, the Röntgen phase was measured to be 3.0 ± 2.1 mrad for a measurement time of 4×10^4 s, which coincides with the expected one of 1.1 mrad within the measured uncertainty under an electric field of $1.92 \text{ kV}/\text{cm}$, a magnetic field of 20 mT, and an interference distance of 17 mm.

DOI: [10.1103/PhysRevA.93.023637](https://doi.org/10.1103/PhysRevA.93.023637)

I. INTRODUCTION

Nowadays, atom interferometry using thermal atomic beams or cold ensembles as atomic sources has become an innovative tool for high-precision measurements of gravity, inertial effect, and fundamental physical constants [1]. It has also become an indispensable tool for highly sensitive measurements of topological phases, such as the Aharonov-Casher phase [2], the scalar Aharonov-Bohm phase [3], and the Berry phase [4], which were observed using a neutron interferometer at the beginning of the verification [5–7]. For example, the Aharonov-Casher effect on a neutral particle with a magnetic moment moving in an electric field was verified with an uncertainty of 1% using atom interferometer experimentally [8,9]. In particular, the Ramsey-Bordé atom interferometer [10] is suitable for measuring the difference between spin-dependent phases, since the particle propagates in a superposition of two spin states [11,12].

In 1993, He and McKellar proposed that there is a dual effect to the Aharonov-Casher effect on a neutral particle with an electric dipole moment interacting with a magnetic field [13]. Independently, Wilkens derived the vector potential when a particle with an electric dipole moment moves in a magnetic field [14]. He called the phase the Röntgen phase for a historical reason and suggested that it be measured using an atom interferometer. Then, Wei *et al.* expanded it to the quantum phase accompanying a neutral particle with an induced dipole in electric and magnetic fields [15]. This vector potential could be measured by an atom interferometer using atoms with polarizability. However, for a long time, the Röntgen phase was not found experimentally and was discussed theoretically as to whether it is a pure quantum effect or a semiclassical local electro-dynamical effect [16].

In 2012, Lepoutre *et al.* succeeded in measuring the Röntgen phase (they called it the He-McKellar-Wilkens phase) using a Li atom interferometer, where the two arms of the interferometer were spatially separated [17]. They used three

standing waves separated by 60 cm as beam splitters for the matter wave and placed two plane capacitors sharing a thin septum during the first and second standing waves, where the two arms were separated by $100 \mu\text{m}$. They verified that the effect is nondispersive [18] and carefully analyzed the behavior both experimentally and theoretically [19,20]. However, the experimental phase shift was still 31% larger than the expected value. In their atom interferometer, the phase resolution was 30 mrad for a measurement time of 20 s and 3 mrad for 2000 s. Therefore, it is important to confirm the Röntgen phase by other methods.

On the other hand, the Ramsey-Bordé atom interferometer is also suitable for the measurement of the Röntgen phase. If we use a superposition of two spin states with different polarizabilities, the Röntgen phase can be measured as the difference between the phases of two wave packets passing through an electrode. In 2006, our group proposed a measurement method of the Röntgen phase using a thermal Ca symmetric Ramsey-Bordé atom interferometer [21]. The estimated value of the Röntgen phase is a few milliradians from the polarizability under the general conditions. However, there were two important problems that had to be addressed to achieve a milliradian phase resolution using our atom interferometer. One problem was the phase stability of the atom interferometer [22] and the other was the perfect recovery of the interference fringes owing to the cancelation of the dispersive Stark effect [23].

In this paper, we report the realization of a milliradian phase resolution by developing a diode laser with a hertz linewidth and a low drift rate. Moreover, we report the perfect recovery of the visibility by using transparent electrodes to apply a constant electric field at the location of the laser beams. Finally, we report our result of the Röntgen phase measured for more than 4×10^4 s using the present system and discuss the performance of this system.

II. PRINCIPLES

A. Röntgen phase

The Lagrangian of neutral particles of mass m , magnetic dipole moment μ , and polarizability α moving with velocity \mathbf{v}

*Present address: Research and Production Corporation, Precision Systems and Instruments, Moscow, 111024 Russia.

†morinaga_a@rs.tus.ac.jp

in an electromagnetic field, specified in the laboratory frame by the electric field strength \mathbf{E} and the magnetic field strength \mathbf{B} , is written using the following equation [14,15]:

$$L = \frac{1}{2}m\mathbf{v}^2 + \boldsymbol{\mu} \cdot \mathbf{B} + \frac{\alpha}{2}(\mathbf{E} + \mathbf{v} \times \mathbf{B})^2 + \mathbf{v} \cdot \frac{\boldsymbol{\mu}}{c^2} \times \mathbf{E}, \quad (1)$$

where c is the speed of light in vacuum. The first term is kinetic energy, the second term is the Zeeman effect, and the last term, called the Aharonov-Casher effect, is a vector potential by which a particle with a magnetic dipole is affected by the electric field without a force, like the Aharonov-Bohm effect of the charged particle. The third term L_3 is related to the polarizability of particles and the electric field with Lorentz correction. The term αB^2 is neglected when compared to the kinetic energy term, after developing the square term in Eq. (1). Then,

$$L_3 \approx \frac{\alpha}{2}\mathbf{E}^2 + \mathbf{v} \cdot (\mathbf{B} \times \alpha\mathbf{E}). \quad (2)$$

The first term is the Stark effect and the second term is another vector potential, namely, the Röntgen phase. It is a duality of the magnetic dipole moment in the electric field and the induced electric dipole moment $\alpha\mathbf{E}$ in the magnetic field. The term yields no force on the particle, but it shifts the phase of the wave function of the particle as

$$\varphi_R = \hbar^{-1} \int d\mathbf{r} \cdot (\mathbf{B} \times \alpha\mathbf{E}). \quad (3)$$

If \mathbf{B} , \mathbf{E} , and \mathbf{v} are perpendicular to each other, it is

$$\varphi_R = \alpha B E D / \hbar, \quad (4)$$

where D is the length of the field where particles pass through. Thus, the Röntgen phase is a nondispersive and pure topological quantum phase.

B. Frequency and phase shift in a Ca atom

Figure 1 shows the energy levels and properties of the related states in a Ca atom. We used two states, namely, the excited 3P_1 , $m = 0$ metastable state with a lifetime of 430 μs and the ground 1S_0 , $m = 0$ state, which are connected by the intercombination line at the wavelength of 657 nm. Both states have no magnetic dipole moment, so that the first-order Zeeman effect and the Aharonov-Casher effect are

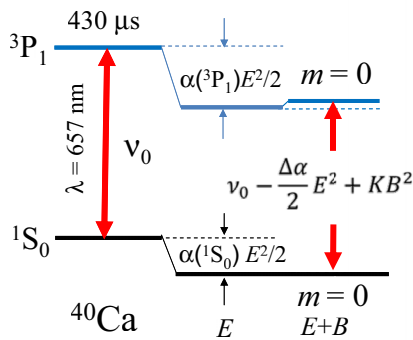


FIG. 1. Intercombination line of Ca atom under electric field E and magnetic field B . α is the polarizability and K is the quadratic coefficient of B .

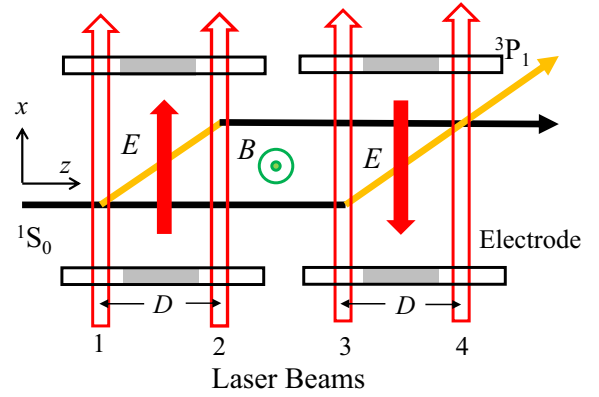


FIG. 2. Symmetrical Ramsey-Bordé atom interferometer with two pairs of electrodes. Atoms in the ground state (1S_0) move to the z direction and interact with four parallel laser beams propagating to the x direction, which are resonant to the transition between the 1S_0 and 3P_1 states. D : beam separation; E : electric field; and B : magnetic field.

not induced. Under a dc electric field, the difference in the polarizabilities between the excited and ground states is $\Delta\alpha = (16.4 \pm 0.3) \times 10^{-40} \text{ F m}^2$ [24], and under a dc magnetic field, the second-order Zeeman coefficient of the 3P_1 , $m = 0$ state attributable to the diamagnetic correction is deduced to be $K = 63.75 \pm 0.09 \text{ Hz/mT}^2$ from theoretical calculation [25]. Under the conditions of $E = 10 \text{ kV/cm}$ and $B = 10 \text{ mT}$, the frequency shifts of the transition between the 3P_1 , $m = 0$ to 1S_0 , $m = 0$ states attributable to the Stark effect and the second-order Zeeman effect are -1.24 MHz and $+6.4 \text{ kHz}$, respectively.

Our atom interferometer is of symmetrical Ramsey-Bordé type with a thermal atomic beam [26], as shown in Fig. 2. Atoms with the velocity v initially in the ground state move to the $+z$ direction and interact with four resonant laser beams, which are copropagating to the x direction. Owing to the energy and momentum exchanges with light during the resonant absorption and the stimulated emission processes, an atomic wave packet coherently splits into the excited and ground states, with different velocities owing to the recoil effect in the x direction. At the zone during the first and second interactions with a laser beam, or the zone during the third and fourth interactions, the wave packet is split into the two states that move in separate directions. When the spaces of the two zones are the same, the atom interferometer is formed. The interference fringes are observed in the fluorescent signal from the excited state. The phase shift is given by [26]

$$\varphi = -\phi_1 + \phi_2 + \phi_3 - \phi_4 + \varphi_q \equiv \Delta\phi + \varphi_q, \quad (5)$$

where ϕ_i is the phase of the i th laser beam. Note that the phase of this atom interferometer does not depend on the laser frequency, in principle. To compose the atom interferometer, the laser frequency is tuned to the resonance frequency under zero electric and magnetic fields. If atoms are perturbed by the electromagnetic field in these zones, the difference φ_q between the phase of the excited state and that of the ground state is created. When the electric field direction is parallel to the light propagation direction and the magnetic field is in

the y direction, the Röntgen phase occurs. From Eq. (4), the Röntgen phase is given by

$$\varphi_R = \frac{\Delta\alpha EBD}{\hbar}, \quad (6)$$

where D is the length of the perturbation. At $v = 750$ m/s and $D = 10$ mm, the phase shifts attributable to the Stark effect, the second-order Zeeman effect, and the Röntgen phase are 10.4 rad, 0.53 rad, and 1.6 mrad, respectively. Thus, the Röntgen phase is very small under normal experimental conditions, in comparison with the other two phases.

C. Measurement principle

For the measurement of the Röntgen phase, the main problem is that the Stark phase shift is dispersive; consequently, the interference signal disappears with a phase shift of more than 2π rad at the thermal atomic beam [23]. Therefore, we put one electrode in the first zone and the other electrode with the same dimension in the second zone. We apply an electric field on them with the same strength but reverse the sign. Then, the Stark phase shift yield at the first zone is canceled out by the opposite Stark phase shift yield at the second zone, so that the interference signal should be recovered. Previously, we tried this method by inserting a steel electrode with a length shorter than the width of the zone (gray parts in Fig. 2), but the interference signal does not recover even at the electric field of few kV/cm, because the strengths of the stray electric field at the locations of the four laser beams were different. It was difficult for us to make the strength of the stray field uniform. Therefore, in this experiment, we aimed at using a transparent electrode with a width larger than the space between two incident laser beams, as shown in Fig. 2. Identically, the electric field will be uniform in the positions between the first (third) and second (fourth) laser beams. In this case, the resonance frequency under the electric field changes owing to the Stark frequency shift; however, the phase of this atom interferometer does not depend on the laser frequency in principle [26].

At the same time, the magnetic field is applied homogeneously to the z direction in all the zones. Then, the phase shift attributable to the second-order Zeeman effect in the first zone is also canceled out by that in the second zone. On the other hand, the Röntgen phase under these configurations becomes twice that of the single electrode, because the sign of the phase shift, which depends on the product of the electric and magnetic field, does not reverse. In the above experiment, we tune the laser frequency to the resonance frequency without an electric field and with the small quantization magnetic field B to select the $m = 0$ state.

III. APPARATUS AND PERFORMANCES

A. Atom interferometer

A schematic of the present experimental setup is shown in Fig. 3. The Ca symmetrical Ramsey-Bordé atom interferometer was almost the same as that described in our previous paper [22]. A thermal Ca atomic beam was generated from an oven with a temperature of 800 °C and was collimated by apertures inserted before and after the interaction region with the laser beams. The vacuum in the chamber was maintained

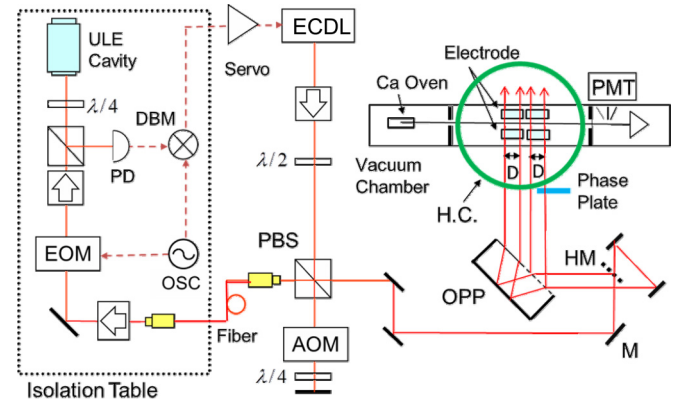


FIG. 3. Experimental setup of the Ca atomic beam apparatus and the atom interferometer using a subhertz linewidth diode laser stabilized to an ultralow-expansion glass (ULE) cavity by the Pound-Drever-Hall method. EOM: electro-optic modulator; PD: photodiode; DBM: double balanced mixer; OSC: oscillator; ECDL: external cavity diode laser; PBS: polarizing beam splitter; AOM: acousto-optic modulator; OPP: optical parallel plate; H.C.: Helmholtz coil; PMT: photomultiplier; M: mirror; HM: half mirror; $\lambda/2$: half-wave plate, and $\lambda/4$: quarter-wave plate.

below 10^{-6} Pa by an ion pump. At 250 mm downstream from the interaction zone, the fluorescence signal from the Ca beam was detected by a photomultiplier tube.

The symmetrical atom interferometer was realized by interaction of four copropagating resonant laser beams perpendicular to the Ca atomic beam with atoms. The output from the diode laser was divided into four copropagating parallel laser beams with equal power by an optical parallel plate with a special coating [26]. Then, the four laser beams were introduced into the interaction zone perpendicular to the atomic beam. The parallelism of the four beams was examined on the basis of the Lamb dip of the resonance line and within $20 \mu\text{rad}$. The separation D between the first two laser beams and the other two laser beams was set to be 8.5 mm. Then, the space between laser beams 2 and 3 was 11.5 mm. The power of each laser beam was adjusted to be 0.6 mW, to maximize the amplitude of interference fringes. A phase shifter made of fused silica was inserted into the path of laser beam 4 to scan the laser phase $\Delta\phi$. A magnetic field of 1.0 mT was applied parallel to the z axis, which was perpendicular to both the atomic beam and the laser beam in the entire interaction zone. The polarization of each laser beam was set parallel to the magnetic field (π polarization) so that the atoms were excited to the $m = 0$ sublevel.

To measure the Röntgen phase, the phase resolution of an atom interferometer should be at milliradian level. As we stated in a previous paper [22], the visibility of the interference fringes decreases as the beam separation increases, because of the laser frequency fluctuation. Therefore, the linewidth of the laser should be less than 16 Hz in $10 \mu\text{s}$. At the same time, to accumulate the signal for a longer integration time, the drift of the laser frequency should be small. Therefore, we improved the linewidth and drift of an external cavity diode laser (ECDL) oscillating at a wavelength of 657 nm by stabilizing to a high-finesse ultralow-expansion (ULE) glass cavity [27] by the Pound-Drever-Hall (PDH) method [28]. Finally, we achieved

a linewidth of less than 1 Hz by evaluating a beat note between two stabilized lasers. We stabilized the ULE glass cavity at a temperature of -3.3°C , where the thermal expansion of the cavity was zero. Then, the linear drift rate of this laser frequency was 14 mHz/s (50 Hz/h) at 1400 days after setup.

By using the above apparatus, the interference fringes were measured. The interaction zone was covered tightly with a lid to keep the atmospheric condition constant, so that the signal fluctuation was reduced. The laser phase was scanned by periodically sweeping the angle of the phase shifter $\Delta\phi$ at 10 Hz, and the interference signals of about two fringes were recorded repeatedly for 40 ms every 100 ms. Sequentially recorded interference fringes for 40 ms were integrated every 20 scans and fitted by the sine function $\sin\{\Delta\phi - \phi(n)\}$ to obtain their phase, where $\phi(n)$ is the initial phase and n is the number of data every 20 scans. The interference fringes were obtained with a constant visibility for a beam interval from 5 to 15 mm. In the present experiment, the oven temperature was reduced to 800°C to maintain a sufficient pressure for the ion pump, so that the visibility was reduced to 10%. Typical interference fringes measured at an integration time of 40 s (0.4 s per point) is shown in Fig. 4(a). The data were fitted by a sine function with a relative standard deviation of 3×10^{-3} . The initial phase was obtained with an uncertainty of 6 mrad.

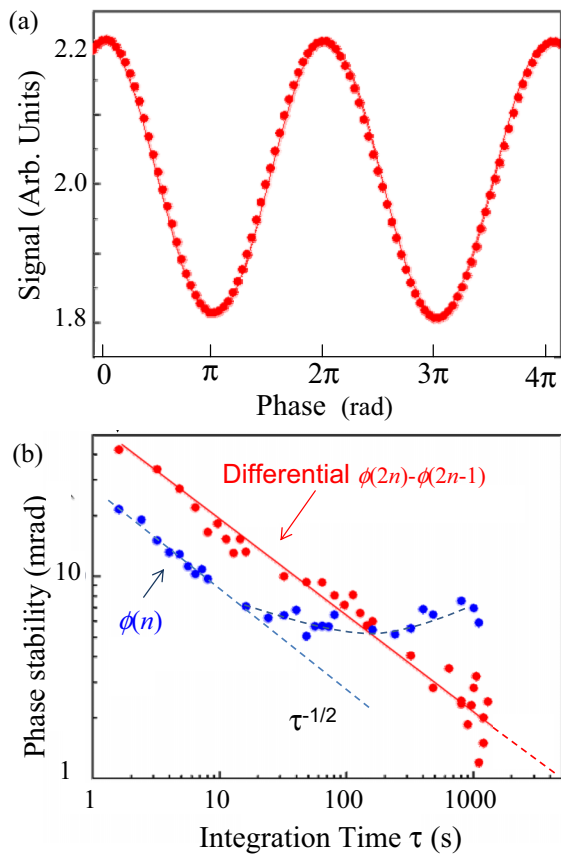


FIG. 4. (a) Interference fringes measured at integration time of 40 s (0.4 s per point). Solid curve is a fitted sine function with a relative standard deviation of 3×10^{-3} . The uncertainty of the phase is 6 mrad. (b) Allan deviation of the phase $\phi(2n) - \phi(2n - 1)$ versus integration time, together with a standard deviation $\phi(n)$. The Allan deviation was deduced from the total data size of 7000 s.

The Allan deviation of the phase was calculated from the data set of the differential initial interference phase $\phi(2n) - \phi(2n - 1)$, in order to remove the drift of the laser phase, which is mainly related to the thermal effect of the phase shifter [22]. The total integration time τ is n times 1.6 s. Figure 4(b) shows a typical Allan deviation of the phase as a function of integration time, together with the simple variance of $\phi(n)$. The simple variance of $\phi(n)$ reaches the minimum value at 10 s and increases owing to the thermal effect of the phase shifter. However, the Allan deviation of the phase decreases according to $\sigma/\text{mrad} = 70/\sqrt{\tau/\text{s}}$, and it is estimated that it will reach 1 mrad at an integration time of 5000 s. In principle, the phase does not depend on the laser frequency; however, the imperfect parallelism will cause the dependence of the phase on the laser frequency. The frequency dependence of the phase was evaluated to be $0.1 \mu\text{rad}/\text{Hz}$, which corresponds to $5 \mu\text{rad}/\text{h}$, for the present drift rate of the laser.

B. ITO electrodes

Previously, we inserted two electrodes with a width of less than D between laser beams 1 and 2, and between 3 and 4. However, each laser beam was affected at different stray fields from the electrodes so that the visibility of the atom interferometer decreased. Therefore, in this experiment, we prepared transparent electrodes using a tin-doped indium oxide (ITO) membrane. The ITO membrane with a thickness of 100 nm was coated on a synthetic quartz optical parallel substrate, together with antireflection (AR) coating. The other surface also has AR coating. The transmission coefficient is 97% at the wavelength of 657 nm. One electrode was composed of two quartz plates that were placed in parallel. The surfaces with depositions of the ITO membrane faced each other at intervals of 5.2 mm. Then, laser beams 1 and 2 were incident on one pair of electrodes and laser beams 3 and 4 were incident on the other pair of electrodes. Each ITO membrane was connected through a Ni-Cr electrode to a high-voltage power supply with a stability of 0.01%. The direction of the electric field in the latter pair was reversed to that in the former pair.

At first, we checked the frequency shift of the Lamb dip for four beams at different strengths of the voltages V owing to the Stark shift as a function of the square of V . The slopes for four laser beams were $(4.6 \pm 0.5) \times 10^{-6} \text{Hz}/\text{V}^2$, $(4.3 \pm 0.5) \times 10^{-6} \text{Hz}/\text{V}^2$, $(5.0 \pm 0.5) \times 10^{-6} \text{Hz}/\text{V}^2$, and $(4.5 \pm 0.5) \times 10^{-6} \text{Hz}/\text{V}^2$ in sequence. The uncertainty depends mainly on the uncertainty of the center of the Lamb dip. When we use the intervals of the electrode (5.2 ± 0.1 mm), we obtain the mean polarizability $\Delta\alpha = (16.5 \pm 1.5) \times 10^{-40} \text{Fm}$, which confirms the reported value [24]. Figure 5(a) shows the interference fringes when the electric field was applied to only one electrode near the oven. The fringes show the phase shift and a decrease in visibility as the strength of the electric field increased. The phase shift varies as a straight line of $(3.3 \pm 0.3) \times 10^{-6} \text{rad cm}^2/\text{V}^2$ as a function of V^2 , as shown in Fig. 5(b). From this value, we could estimate the velocity of the Ca atom at 800°C as $750 \pm 100 \text{m/s}$. The visibility at an electric field of 2 kV/cm decreased to 50% of that at zero electric field.

When we applied a voltage of 2.000 kV ($E = 3.85 \pm 0.08 \text{kV}/\text{cm}$) to the electrode near the detector and gradually

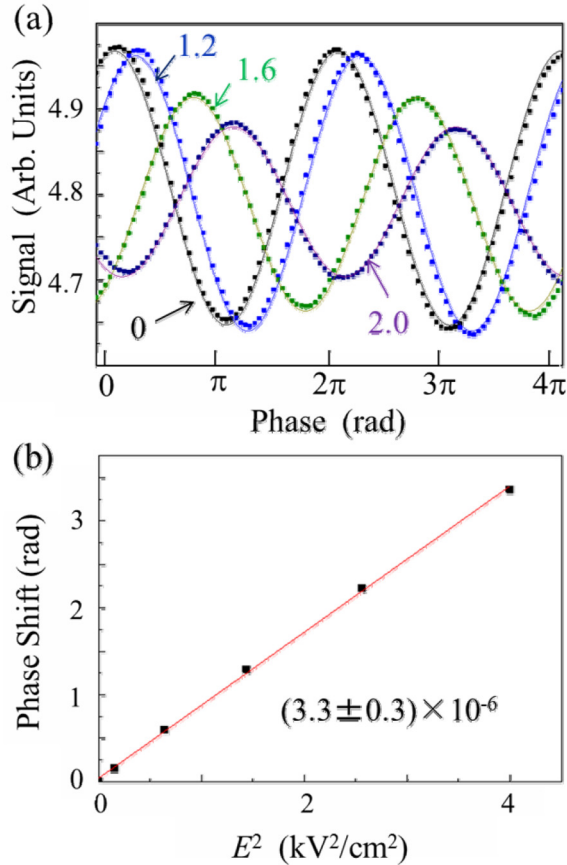


FIG. 5. (a) Interference fringes under different electric fields. Figures are the strength of electric field in kV/cm. (b) Observed phase shift versus square of electric field.

changed the voltage applied to the other electrode from 1.8 kV towards 2 kV, the visibility of the interference fringes increased and recovered at 1.955 kV to the original value with zero electric field, as shown in Fig. 6. The difference of 0.045 kV between the two voltages shows that the interval difference between the two electrodes was within the uncertainty of 0.1 mm. This perfect recovery was ascertained up to an electric

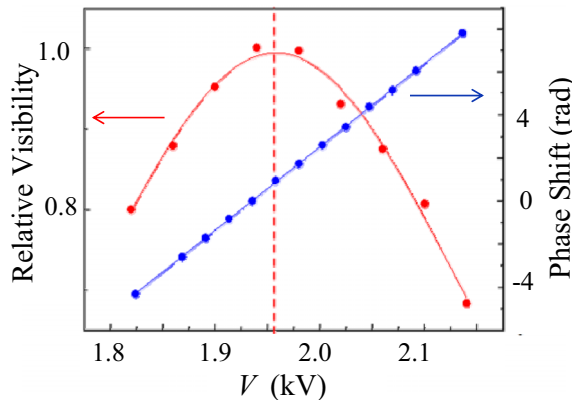


FIG. 6. Recovery of visibility due to the cancelation of the Stark phase shift. A voltage of 2.000 kV was applied to one electrode and the phase shift was canceled out when 1.955 kV was applied to the other electrode.

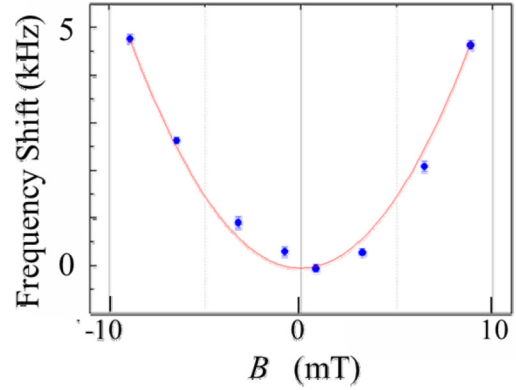


FIG. 7. Second-order Zeeman frequency shift with a fitted parabolic curve.

field of 10 kV/cm. At the same time, a small residual phase shift occurs according to the difference between the strengths of the electric fields of the two electrodes. The degree was 1 mrad for the stability of the present electric field of 0.1 V/cm.

C. Magnetic field

In the entire region of the atom interferometer, a uniform magnetic field was applied by a Helmholtz coil perpendicular to the electric field direction and the propagation direction of the thermal atomic beam. The strength of the magnetic field was calibrated using the first-order Zeeman frequency shift between the $S, m = \pm 1$ and $P, m = 0$ states. The second-order Zeeman frequency shift between the $S, m = 0$ and $P, m = 0$ states was measured using the Ramsey fringes of the Ca atom as a parabolic function of the magnetic field strength, as shown in Fig. 7. The frequency shift is $\Delta\nu = (60.3 \pm 3.0) \times B^2$ Hz/mT² (B is in mT), which confirms the theoretical value attributable to the diamagnetic correction [25].

The phase shift attributable to the second-order Zeeman effect should be canceled under a uniform magnetic field in the entire interferometry region. However, when the magnetic field of 10 mT was applied to the atom interferometer, a phase shift of about 10 mrad was observed with a slow rise-up time of 5 min. The phase shift will occur owing to the spatial inhomogeneity of the magnetic field because of the misalignment of the coils and the thermal expansion of the coils with high current. Although this degree was much larger than the expected Röntgen phase, the value was the same, regardless of the sign of the magnetic field. Actually, we measured the phase variation with +10 and -10 mT, alternatively. The mean values of the phase were the same within the uncertainty, as shown in Fig. 8. Therefore, we can measure further twice the Röntgen phase by measuring the difference in the phase shifts with positive and negative magnetic fields under the same electric field. Finally, we measured the phase stability under the magnetic field of +10 mT and we obtained almost the same stability as that without the magnetic field.

IV. MEASUREMENT OF RÖNTGEN PHASE

In Fig. 4(b), we showed that the phase of the interference fringes drifts with time because of the thermal effect, so that we cannot accumulate the signal of the interference fringes.

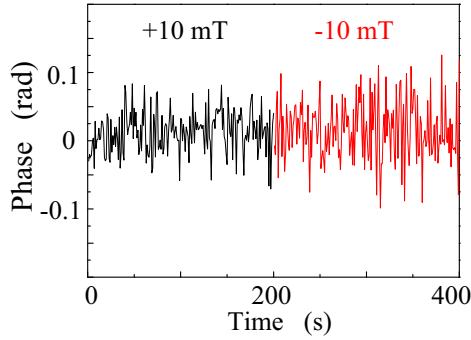


FIG. 8. Phase fluctuations under magnetic field measured from a few minutes after switch-on. The first half: +10 mT; the last half: -10 mT.

However, we could obtain the phase without drift by making the difference between two adjacent samples of variation.

Our strategy for the measurement of the Röntgen phase is shown in Fig. 9(a). During the first measurement period of 20 000 s, a magnetic field of $+10.0 \pm 1.0$ mT was applied to the interaction zone. After turning on the magnetic field, we waited five minutes for warm-up of apparatus and 20 measurement cycles (~ 20 s) were carried out without an electric field. Then, an electric field of 1.92 ± 0.04 kV/cm was applied to the electrodes. After 10 s for charging electrodes, 20 measurement cycles were carried out. Then, the electric field was turned off. After 20 s for discharging electrodes, the next measurements were started. These processes were repeated for about 20 000 s. Then the magnetic field was quickly reversed to -10.0 ± 1.0 mT. Then, the second sequence of the measurement was carried out for 20 000 s.

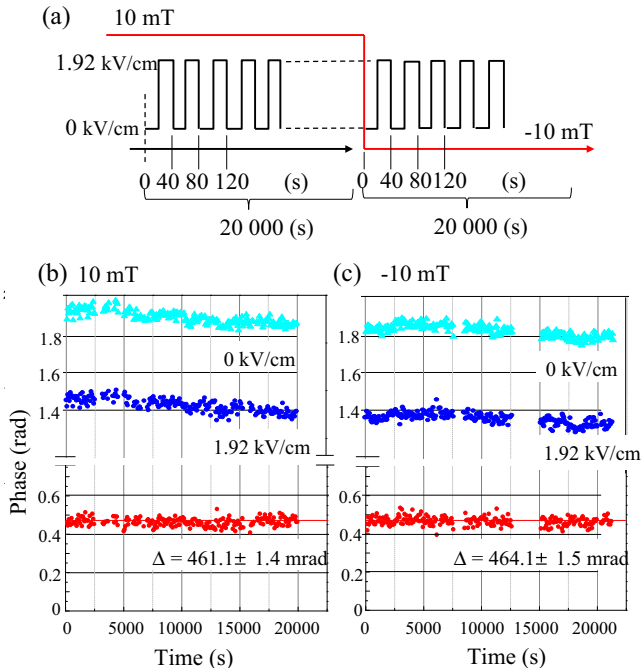


FIG. 9. (a) Timing diagram of the measurement. Waiting times are excluded. (b) Phase shifts of 0 kV/cm, 1.92 kV/cm, and difference under 10 mT. (c) Phase shifts of 0 kV/cm, 1.92 kV/cm, and difference under -10 mT.

Figures 9(b) and 9(c) show the results with magnetic fields of +10 and -10 mT, respectively, as a function of time. The upper dots indicate the phase shift without electric field and the middle dots indicate the phase shift with an electric field of 1.92 kV/cm. Both data vary in the same way as a function of time. Therefore, in the bottom dots, which indicate the difference between both dots, the variations are removed. It should be noted that the differences are distributed about their mean values. The mean and variance of the phases in the bottom dots with +10 and -10 mT are 461.1 ± 1.4 and 464.1 ± 1.5 mrad, respectively.

Their difference of 3.0 ± 2.1 mrad corresponds to the Röntgen phase for $E = 1.92 \pm 0.04$ kV/cm, $B = 20.0 \pm 1.4$ mT, and $D = 17 \pm 1$ mm. The expected value for the Röntgen phase is 1.1 ± 0.1 mrad. Thus, our first experimental value just coincides with the expected value within the measurement uncertainty. However, the previously determined discrepancy between the experimental and theoretical values [19,20] cannot be resolved with this uncertainty. The main source of the present uncertainty is the statistical uncertainty of the phase. In order to reduce the statistical uncertainty, the visibility of the interference fringes should be increased, in addition to an increase in the measurement period. One attractive way to increase the visibility will be a velocity selection of the thermal atomic beam besides a careful alignment of the interferometer [26].

To measure more definitely the Röntgen phase and dependence on the electric field, we tried to apply a higher electric field to the ITO electrodes. However, if we apply an electric field higher than 6 kV/cm, a large drift of more than 10 mrad appeared in the phase, apart from the drift observed without electric field. The magnitude of the drift becomes larger as the strength of the electric field increases. Therefore, we must try to pursue the causes of drift and remove them in order to measure the Röntgen phase for a higher electric field.

V. CONCLUSIONS

We have developed a thermal Ca atom interferometer with a milliradian phase resolution using a subhertz linewidth diode laser. The Allan deviation of the phase fluctuation decreases according to $\sigma/\text{mrad} = 70/\sqrt{\tau/\text{s}}$ and reaches 1 mrad at the integration time of 5000 s. We have developed an ITO transparent electrode with a transmittance of 97% and canceled out the Stark effect using two electrodes with the reversed direction of the electric field. We measured the polarizability and the second-order Zeeman coefficient between the 3P_1 , $m = 0$ and 1S_0 , $m = 0$ states. The dependence of the phase on the fluctuation of the laser frequency was $0.1 \mu\text{rad}/\text{Hz}$ and that on the fluctuation of the electric field was $10 \text{ mrad}/(\text{V}/\text{cm})$.

Finally, using this atom interferometer, we measured the Röntgen phase under an electric field of 1.92 kV/cm, a magnetic field of 20 mT, and an interference distance of 17 mm. The obtained phase shift is 3.0 ± 2.1 mrad, which just coincides with the expected value of 1.1 mrad. At an electric field higher than 6 kV/cm, however, a drift of the phase was observed as a function of time. To investigate the previously determined discrepancy between the experimental and theoretical values [19,20], hereafter we shall try to remove the cause of the drift about the ITO electrodes and to measure

the Röntgen phase under an electric field higher than 2 kV/cm with an uncertainty of 1 mrad.

ACKNOWLEDGMENTS

We thank Dr. Kazuhito Honda for his contribution during the initial stage of this study and Dr. Tomoya Akatsuka and Shu

Hirata for their considerable contributions to the development of the milliradian laser system, and Nobuhiko Sone for his effort in the analysis of laser fluctuation. This research was partially supported by a Grant-in-Aid for Scientific Research on Innovative Areas “Extreme quantum world opened up by atoms” (Grant No. 21104006) from the Ministry of Education, Culture, Sports, Science, and Technology, Japan.

-
- [1] A. D. Cronin, J. Schmiedmayer, and D. E. Pritchard, *Rev. Mod. Phys.* **81**, 1051 (2009).
- [2] Y. Aharonov and A. Casher, *Phys. Rev. Lett.* **53**, 319 (1984).
- [3] Y. Aharonov and D. Bohm, *Phys. Rev.* **115**, 485 (1959).
- [4] M. V. Berry, *Proc. R. Soc. London, Ser. A* **392**, 45 (1984).
- [5] A. Ciminno, G. I. Opat, A. G. Klein, H. Kaiser, S. A. Werner, M. Arif, and R. Clothier, *Phys. Rev. Lett.* **63**, 380 (1989).
- [6] B. E. Allman, A. Ciminno, A. G. Klein, G. I. Opat, H. Kaiser, and S. A. Werner, *Phys. Rev. Lett.* **68**, 2409 (1992).
- [7] T. Bitter and D. Dubbers, *Phys. Rev. Lett.* **59**, 251 (1987).
- [8] K. Zeiske, G. Zinner, F. Riehle, and J. Helmcke, *Appl. Phys. B: Lasers Opt.* **60**, 205 (1995).
- [9] S. Yanagimachi, M. Kajiro, M. Machiya, and A. Morinaga, *Phys. Rev. A* **65**, 042104 (2002).
- [10] Ch. J. Bordé, *Phys. Lett. A* **140**, 10 (1989).
- [11] K. Numazaki, H. Imai, and A. Morinaga, *Phys. Rev. A* **81**, 032124 (2010).
- [12] A. Morinaga and Y. Hasegawa, *Phys. Rev. A* **92**, 013403 (2015).
- [13] X.-G. He and B. H. J. McKellar, *Phys. Rev. A* **47**, 3424 (1993).
- [14] M. Wilkens, *Phys. Rev. Lett.* **72**, 5 (1994).
- [15] H. Wei, R. Han, and X. Wei, *Phys. Rev. Lett.* **75**, 2071 (1995).
- [16] S. A. R. Horsley, and M. Babiker, *Phys. Rev. Lett.* **95**, 010405 (2005).
- [17] S. Lepoutre, A. Gauguet, G. Tréneç, M. Büchner, and J. Vigué, *Phys. Rev. Lett.* **109**, 120404 (2012).
- [18] J. Gillot, S. Lepoutre, A. Gauguet, M. Büchner, and J. Vigué, *Phys. Rev. Lett.* **111**, 030401 (2013).
- [19] S. Lepoutre, A. Gauguet, M. Büchner, and J. Vigué, *Phys. Rev. A* **88**, 043627 (2013).
- [20] S. Lepoutre, J. Gillot, A. Gauguet, M. Büchner, and J. Vigué, *Phys. Rev. A* **88**, 043628 (2013).
- [21] K. Honda, J. Ichimura, N. Sone, and A. Morinaga, *Book of Abstracts for the XX International Conference on Atomic Physics* (Institute for Quantum Optics and Quantum Information, Innsbruck, 2006), p. 246.
- [22] T. Akatsuka, Y. Mori, N. Sone, Y. Ohtake, M. Machiya, and A. Morinaga, *Phys. Rev. A* **84**, 023633 (2011).
- [23] A. Morinaga, M. Nakamura, T. Kurosu, and N. Ito, *Phys. Rev. A* **54**, R21 (1996).
- [24] K. Zeiske, Report No. PTB-Bericht, PTB-Opt-48 (Physikalisch-Technische Bundesanstalt, Braunschweig, Germany, 1995), p. 39.
- [25] N. Beverini, E. Maccioni, and F. Strumia, *J. Opt. Soc. Am. B* **15**, 2206 (1998).
- [26] S. Yanagimachi, Y. Omi, and A. Morinaga, *Phys. Rev. A* **57**, 3830 (1998).
- [27] S. Hirata, T. Akatsuka, Y. Ohtake, and A. Morinaga, *Appl. Phys. Exp.* **7**, 022705 (2014).
- [28] R. W. P. Drever, J. H. Hall, F. V. Kowalski, J. Hough, G. M. Ford, A. J. Munley, and H. Ward, *Appl. Phys. B* **31**, 97 (1983).